1-1-2016

Rapidly evolving ultrafine and fine mode biomass smoke physical properties: Comparing laboratory and field results

Christian M. Carrico
New Mexico Institute of Mining and Technology

Anthony J. Prenni
US National Park Service

Sonia M. Kreidenweis
Colorado State University

Ezra J.T. Levin
Colorado State University

Christina S. McCluskey
Colorado State University

See next page for additional authors

AGU PUBLICATIONS

JGR

Journal of Geophysical Research: Atmospheres

RESEARCH ARTICLE
10.1002/2015JD024389

Key Points:
- Quickly evolving biomass smoke size and optical properties are largely driven by combustion efficiency
- Flaming combustion favors high concentrations of light absorbing particles with diameter ~50 nm
- Smoldering combustion favors larger diameter, highly light scattering aerosols

Correspondence to:
C. M. Carrico,
carrico@nmt.edu

Citation:
Carrico, C. M., A. J. Prenni, S. M. Kreidenweis, E. J. T. Levin, C. S. McCluskey, P. J. DeMott, G. R. McMeeking, S. Nakao, C. Stockwell, and R. J. Yokelson (2016), Rapidly evolving ultrafine and fine mode biomass smoke physical properties: Comparing laboratory and field results, *J. Geophys. Res. Atmos.*, *121*, 5750–5768, doi:10.1002/2015JD024389.

Received 22 OCT 2015
Accepted 25 APR 2016
Accepted article online 28 APR 2016
Published online 14 MAY 2016

Rapidly evolving ultrafine and fine mode biomass smoke physical properties: Comparing laboratory and field results

Christian M. Carrico[1], Anthony J. Prenni[2], Sonia M. Kreidenweis[3], Ezra J. T. Levin[3], Christina S. McCluskey[3], Paul J. DeMott[3], Gavin R. McMeeking[4,5], Shunsuke Nakao[6], Chelsea Stockwell[7], and Robert J. Yokelson[7]

[1]New Mexico Institute of Mining and Technology, Socorro, New Mexico, USA, [2]U.S. National Park Service, Lakewood, Colorado, USA, [3]Colorado State University, Fort Collins, Colorado, USA, [4]Droplet Measurement Technologies, Inc., Boulder, Colorado, USA, [5]Now at Handix Scientific, Boulder, Colorado, USA, [6]Clarkson University, Potsdam, New York, USA, [7]Department of Chemistry, University of Montana, Missoula, Montana, USA

Abstract Combining field and laboratory results, we present biomass smoke physical properties. We report sub-0.56 μm diameter (D_p) particle sizing (fast mobility particle sizer, FMPS) plus light absorption and scattering at 870 nm (photoacoustic extinctiometer). For $D_p < 200$ nm, the FMPS characterized sizing within ±20% compared to standards. As compared to the traditional scanning mobility particle sizer, the FMPS responded most accurately to single-mode polydispersions with mean $D_p < 200$ nm, which characterized the smoke sampled here. Smoke was measured from laboratory fresh emissions (seconds to hours old), the High Park Fire (hours to < 1 day), and from regional biomass burning (several days). During a High Park Fire episode, light extinction rapidly reached a maximum of $\sigma_{ep} = 569 \pm 21$ Mm^{-1} (10 min) with aerosol single scattering albedo peaking at $\omega = 0.955 \pm 0.004$. Concurrently, number concentration and size peaked with maximum $D_p = 126$ nm and a unimodal distribution with $\sigma_g = 1.5$. Long-range transported smoke was substantially diluted (N_{tot} factor of 7 lower) and shifted larger (maximum $D_p = 143$) and wider ($\sigma_g = 2.2$). We compared ambient data to laboratory burns with representative western U.S. forest fuels (coniferous species Ponderosa pine and Alaska black spruce). Smoldering pine produced an aerosol dominated by larger, more strongly light scattering particles ($D_p > 100$ nm), while flaming combustion produced very high number concentrations of smaller ($D_p \sim 50$ nm) absorbing particles. Due to smoldering and particle growth processes, D_p approached 100 nm within 3 h after emission. Increased particle cross-sectional area and Mie scattering efficiency shifted the relative importance of light absorption (flaming maximum) and light scattering (smoldering maximum), increasing ω over time. Measurements showed a consistent picture of smoke properties from emission to aging.

1. Introduction

A changing relationship between wildland fire and human civilization is an important intersection of issues between land use, climate change, and air quality [*Rocca et al.*, 2014]. Biomass smoke in the atmosphere originates from multiple sources including agricultural burning, residential home heating and cooking fires, and prescribed and wildland fires. Increases in biomass smoke emissions, a major source of both particulate material (PM, where $PM_{2.5}$ is the fraction of PM with aerodynamic diameters less than 2.5 μm) and greenhouse gases, are emerging concerns for impacts on atmospheric chemistry, visibility, cloud nucleation, climate interactions, human health, and regulatory compliance [*Kaufman and Fraser*, 1997; *Naeher et al.*, 2007; *Watson*, 2002].

Biomass smoke from wildland fire is a developing air quality concern in many regions globally and particularly in the U.S. mountain west where episodic impacts extend across wide regions [*Kreidenweis et al.*, 2001; *McMeeking et al.*, 2006; *Wotawa and Trainer*, 2000]. A study by *Spracklen et al.* [2007] concluded that summer wildfires are the most important driver of interannual variability in observed total carbonaceous PM across the continental U.S. A modeling study by *Park et al.* [2007] attributed 50% of U.S. annual mean particulate carbon concentrations to biomass burning. A projection of the impacts of climate change on biomass burning predicts an increase of 54% in average annual burned area in the western U.S. by midcentury, further underscoring a growing importance of smoke [*Spracklen et al.*, 2009]. Tied to the predicted shifts with continued climate change, such trends are strongly linked to burn season length and regional drought conditions

[*Westerling et al.*, 2006]. The improvements in air quality due to anthropogenic emission reductions are at risk from the counteracting influence of increasing wildland fire emissions, particularly related to $PM_{2.5}$ and O_3 issues [*Val Martin et al.*, 2015].

Consistent with predictions, recent U.S. wildland fire statistics indicate that U.S. wildfires are becoming fewer in number though larger in acreage (www.nifc.gov) compared with twentieth century data. Average acres per fire were 30 ± 13 during 1960–1999 versus 89 ± 31 during 2000–2014. Total U.S. wildland fire acreage burned per year totals $3.9 \pm 1.5(10)^4$ versus $6.6 \pm 2.4(10)^4$ km^2 for the respective periods, including six recent years that have exceeded the 1960–1999 mean by three standard deviations. A trend toward higher-intensity, larger-scale, crowning fires has vital ecological implications for forest and soil health [*Certini*, 2005]. Recent fire history implicates fire management practices of the twentieth century as well as recent climatic changes as contributing factors [*Pierce et al.*, 2004; *Veblen et al.*, 2000; *Williams et al.*, 2010]. Thus, concern over biomass smoke emissions centers on both current emissions and likely future trends given recent wildfire behavior and continued climate changes [*Westerling et al.*, 2006].

Biomass burning emits numerous gas phase species including carbon monoxide (CO), carbon dioxide (CO_2), nitrogen oxides (NO_x), and volatile organic compounds (VOCs) [*Andreae and Merlet*, 2001]. With the release of these precursors, biomass burning leads to net ozone (O_3) production, though individual plumes can also be an O_3 sink depending on their NO to NO_2 ratio and attenuation of UV radiation among other factors [*Jaffe et al.*, 2008]. Atmospheric particulate contributions are both primary and secondary. Biomass burning is a major global source of particulate organic carbon (OC), elemental carbon (EC), "brown" carbon that absorbs radiation at shorter wavelengths, and inorganic species [*Bond et al.*, 2013; *Saleh et al.*, 2014]. Tar balls generated via volatilization are a constituent of biomass smoke; they are somewhat spherical "brown carbon" particles, absent the fractal structures of sooty agglomerates though with wavelength-dependent light absorbing properties [*Hand et al.*, 2005; *Posfai et al.*, 2004; *Toth et al.*, 2014].

Smoke aerosol microphysical properties and composition play a vital role in determining the nature and severity of air quality and climate impacts [*Reid et al.*, 2005a, 2005b]. Particle size distribution and radiative properties are key variables in determining smoke impacts on human health, visibility, climate, and compliance with regulatory requirements. For example, particle growth into a range with higher Mie scattering efficiency results in higher light scattering efficiency, greater cross-sectional area, and thus greater contribution to haze. Furthermore, particle size distributions relate strongly to human exposure and play an important role in cloud nucleation. Historically, $PM_{2.5}$ has been the focus of air quality regulations. However, increased attention has been focused on the role of ultrafine particles (PM with $D_p < 100$ nm), particularly in relation to human health [*Pope and Dockery*, 2006].

The overall intent of this study is to incorporate observations of freshly emitted biomass smoke, with a focus on the ultrafine and fine mode aerosols which dominate the number distributions. Comprehensive comparisons of particle and gas phase emission factors from biomass smoke field and laboratory studies are provided elsewhere [*McMeeking et al.*, 2009; *Yokelson et al.*, 2013]. Previous studies have integrated measurements of the coarse mode with accumulation mode generated from biomass burning [*Levin et al.*, 2010]. From this series of biomass experiments, we examine aerosol temporal evolution, using a common set of instruments for direct measurement intercomparability [*Price et al.*, 2014]. In particular, this study examines the relationship between sizing parameters and optical properties in relation to combustion and environmental conditions that are controlling variables. Synthesis yields new insights on biomass smoke properties using results from the laboratory and wildland fires.

2. Experimental Details

Measurements were conducted during three events: a laboratory biomass burning experiment (The Fire Lab at Missoula Experiment-4, FLAME-4) in October–November 2012, ambient measurements during the High Park Fire in Colorado, and ambient measurements of long-range transported smoke arriving in northern Colorado from the northwest U.S. The experiments provide a unique opportunity to examine real-world western U.S. biomass smoke properties compared with representative laboratory measurements using the same measurement techniques. The following describes the measurement campaigns, detailed measurement techniques, and experimental quality assurance efforts.

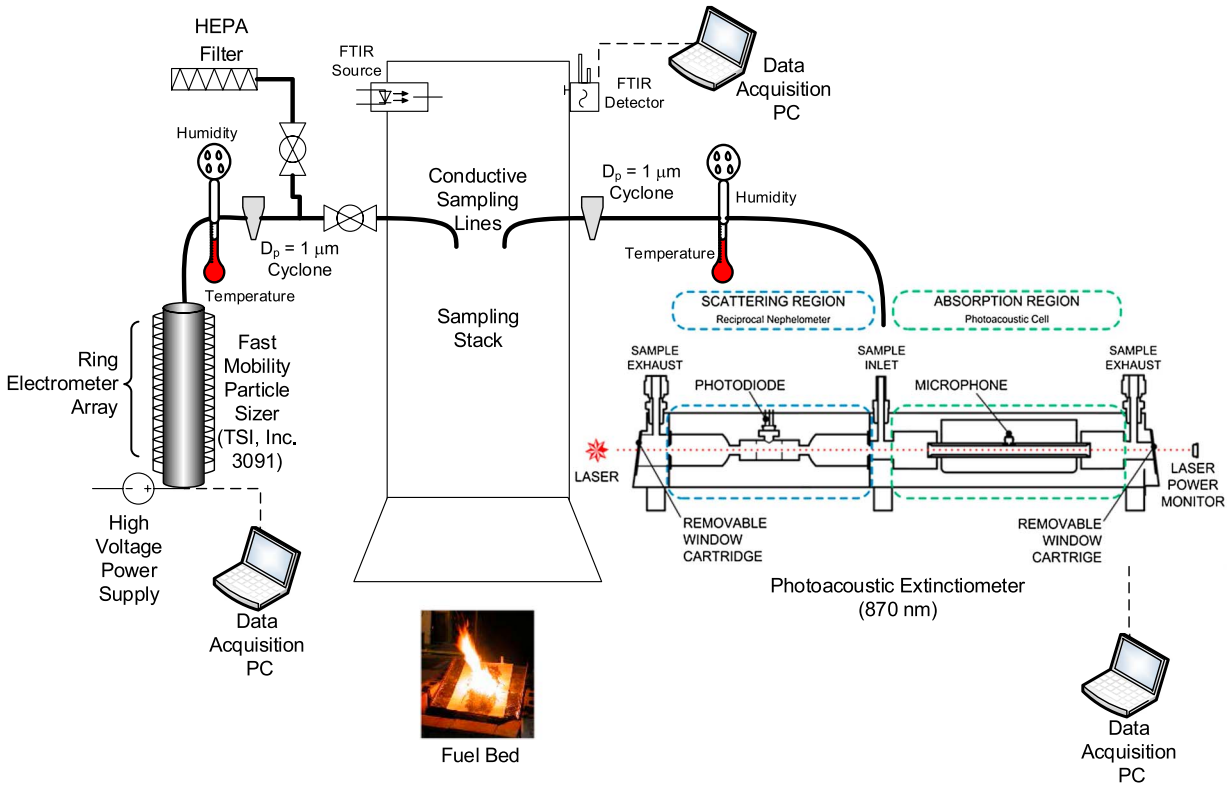

Figure 1. Experimental setup showing sampling strategy for laboratory combustion experiments including sample lines (solid dark lines) and data flow (dashed line) (FLAME-4).

2.1. Laboratory Measurement Campaign Details

The FLAME-4 experiment, conducted in October–November 2012 at the U.S. Department of Agriculture/U.S. Forest Service Missoula Fire Sciences Laboratory in Missoula, Montana, used controlled combustion conditions [*Stockwell et al.*, 2014]. More details on the combustion facility are found in *Christian et al.* [2003, 2004]. A diagram of the experimental setup for a typical "stack" burn is shown in Figure 1, and relevant measurement technique details will be described further below. For "stack burns," sampling occurred through an exhaust mixing stack approximately 16.5 m above the burn platform during combustion. For "room burns," smoke from the fire was allowed to first fill the 3600 m^3 combustion chamber, and sampling occurred over a 3–4 h period in an adjacent laboratory [*McMeeking et al.*, 2009].

We selected representative experiments from the FLAME-4 study focusing on those with continuous records from all instruments where detection or saturation limits were not challenged. Among FLAME-4 experiments, two western U.S. fuels were examined: Alaska black spruce (*Picea mariana*) and Ponderosa pine (*Pinus ponderosa*). Alaska black spruce is a coniferous species common in the northern U.S., Canada, and Alaska. Fuel composition was mostly carbon (50.5%) with small contributions from hydrogen (6.4%), nitrogen (0.7%), sulfur (0.05%), nondetect for chlorine and 3.5% residual ash. Due to its relevance and ample data, we also focus on Ponderosa pine, the most prevalent species of pine in the western U.S. and taken from near Missoula, Montana [*Safford*, 2013]. It is a species that is fire adapted and proliferates with recurrence of low-intensity fires [*Kershaw et al.*, 1998]. Fire regimes of Ponderosa pine have been altered by a range of activities including fire suppression, agriculture, grazing, and climate change [*Noss et al.*, 2006; *Pierce et al.*, 2004; *Veblen et al.*, 2000; *Williams et al.*, 2010]. Chemical analysis of Ponderosa pine showed composition dominated by carbon (51.1%) with small contributions from hydrogen (6.6%), nitrogen (1.1%), nondetects for chlorine and sulfur, and 1.5% residual ash. Average moisture contents of the fuels were 77 ± 16% for pine and 34 ± 17% for spruce. The likely remaining fractions of each fuel consisted of oxygen and trace species.

Table 1. Smoke Measurement Sampling Conditions Expressed as Arithmetic Mean ± Standard Deviation

Measurement Period	Instrument	RH (%)	Temperature (°C)	Pressure (mB)
FLAME Burn 070	FMPS	12.1 ± 0.2	29.7 ± 0.1	865 ± 1
	PAX	12.4 ± 0.3	31.9 ± 0.1	891 ± 3
13 June 2012	FMPS	19.0 ± 4.0	27.4 ± 0.4	844 ± 3
	PAX	24.4 ± 3.5	23.2 ± 1.6	827 ± 3
14–15 August 2012	FMPS	28.0 ± 5.0	26.8 ± 0.8	823 ± 1

All laboratory smoke measurements were sampled undiluted into the instruments, although the smoke plume sampled 16.5 m above the fire had been mixed with room air from its emission point to its sampling point. Measured sampling conditions including relative humidity (RH), dry bulb temperature and pressure are given for Burn 070 in Table 1 and other burns were similar to that shown. Sample temperature was slightly above ambient and sample pressure was slightly below ambient. Relative humidity is an important parameter as it will affect water uptake as smoke with a substantial inorganic component are hygroscopic. For our purposes, sampling conditions here (RH < 30%) are considered "dry," as hygroscopic growth factors were found to be <1.02 for such low humidities [*Carrico et al.*, 2010]. For laboratory experiments we had a direct indicator of combustion efficiency from FTIR measurements of CO and CO_2 [*Stockwell et al.*, 2014]. The modified combustion efficiency is expressed as MCE = excess CO_2/(excess CO_2 + excess CO) where "excess" indicates the concentration above room background [*Yokelson et al.*, 1996].

2.2. Field Measurement Campaign

We compare the measured laboratory-generated fresh biomass smoke to ambient biomass smoke. As a case study of smoke impacts (as indicated by elevated carbon monoxide), we examine the High Park Fire near Fort Collins, CO. The High Park Fire in the Roosevelt National Forest began on 9 June 2012, with full containment on 1 July 2012. The fire was the second most damaging wildfire in Colorado history at the time, burning over 350 km^2, causing one fatality and destruction of 259 homes, and costing over $39 million in fire suppression costs (www.inciweb.org). The High Park Fire burned in the mountains to the northwest of Fort Collins, at an altitude spanning an approximate range of 1600 m to over 3100 m and above the populated Colorado Front Range (CFR) cities such as Fort Collins (~1500 m). Severe episodic smoke impacts on air quality resulted, at times affecting hundreds of thousands of residents in Fort Collins and along the CFR [*McCluskey et al.*, 2014].

A second period examined and impacted by biomass smoke transported over longer distances occurred on 14–15 August 2012. The National Interagency Fire Center data showed mid-August 2012 to be an extremely active fire period in western U.S., with a lack of activity in Colorado (www.inciweb.gov). In the western U.S., 15,000 km^2 burned in August 2012 (largest August on record), with major events in Northern California/Nevada including the Chips (300 km^2), and Rush (1,270 km^2) fires, and in Idaho/Western Montana including the Mustang Complex (1020 km^2), Trinity Ridge (590 km^2), and Halstead (570 km^2) fires, and numerous, smaller regional fires (https://www.ncdc.noaa.gov/sotc/fire/201208) [*NOAA,* 2012]. Ensemble isentropic air mass back trajectories using HYSPLIT (not shown here) and run for 96 h prior to arrival in Colorado showed westerly flow, some passing over the active fire region. Analysis of MODIS satellite data pointed to the influence of these Northwestern U.S. fires as well [*Val Martin et al.*, 2013]. Consistently, the U.S. Naval Research Laboratory (NRL) US Navy Aerosol Analysis and Prediction System (NAAPS) model showed a large spatial extent of smoke extending to Colorado from Northwestern U.S. fires on 15 August 2012 (http://alg.umbc.edu/usaq/images/nrl-20120815.jpg).

Ambient measurement sites were located in west Fort Collins (Colorado State University, CSU, foothills campus), central Fort Collins (CSU main campus), east Fort Collins, and in Loveland, CO, (approximately 4 km ESE, 9 km ESE, 14 km ESE, and 20 km SSE of the fire's southeast extent, respectively) (Figure 2). For all ambient measurements, each instrument operated on its own inlet at its respective site. During data collection, all instruments were time synchronized to local standard time (or LST for Mountain time zone) using hour ending time stamps.

2.3. Light Extinction Measurements

We measured particle light scattering and absorption coefficients (σ_{sp} and σ_{ap}) at a frequency of 1 Hz with a photoacoustic extinctiometer (PAX, Model 870 nm, DMT, Inc.), sampling at a flow rate of approximately 1 lpm

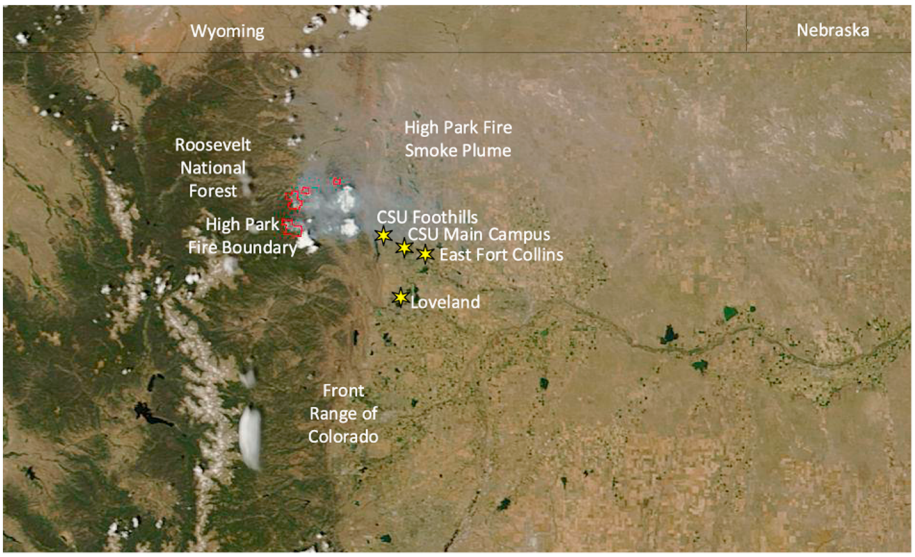

Figure 2. Locations of ambient sampling sites with respect to the High Park Fire in Colorado in June 2012. Image of the High Park Fire boundary and smoke plume from NASA MODIS satellite. Background image from Google Earth.™

[*Arnott et al.*, 1999; *Nakayama et al.*, 2015]. Derived from the instrument measurement is the aerosol single scattering albedo or SSA ($\omega = \sigma_{sp}/[\sigma_{sp} + \sigma_{ap}]$). The instrument sampled through a 0.6 cm outer diameter (OD) electrically conductive sampling line, approximately 3 m in length (residence time, $\tau < 3$ s) with no further sample conditioning. The PAX was calibrated by first using a predominantly light scattering aerosol, $(NH_4)_2SO_4$ with complex refractive index of $1.52 \pm 0.01 + 0.00i \pm 0.03$ at 532 nm [*Lang-Yona et al.*, 2009], followed by a strongly absorbing aerosol (propane torch soot). Calibrations compared measured light scattering and absorption to directly measured light extinction applying the Beer-Lambert Law to laser intensity attenuation in the optical cavity [*Arnott et al.*, 2000]. The calibration is not sensitive to the optical properties of the calibration material (e.g., size and refractive index) because extinction is determined directly from the Beer-Lambert Law. Minor uncertainties are introduced when applying the calibrated response to ambient data due to the fixed geometry of the measurement cell and differences in the scattering phase function for different aerosols. See *Nakayama et al.* [2015] for a detailed treatment. During measurements, the instrument autozeroed periodically by switching a particle filter in line.

2.4. $PM_{2.5}$ Mass Concentrations and Related Gas Phase Species Concentrations

For ambient measurements during the High Park Fire, additional $PM_{2.5}$ and gas phase species are examined here to contextualize sizing and optical measurements. $PM_{2.5}$ mass concentrations were measured at the foothills site with a beta attenuation monitor (Met One, Inc. BAM 1020). The BAM $PM_{2.5}$ mass measurement relies on attenuation of beta radiation through a filter deposit and reports 1 h time resolution $PM_{2.5}$ mass concentrations. In order to monitor worker smoke exposure and adjust work scheduled during the High Park Fire, the BAM 1020 was operated indoors on the CSU Foothills campus near the fire's southeast boundary. The BAM instrument flow was measured and verified during sampling using an external audit flow standard device ($Q = 16.4$ lpm versus nominal 16.7 lpm). After the field measurements, sampling using an external high-efficiency particulate-free air (HEPA) filter device showed $PM_{2.5}$ concentration on zero air of -3.0 ± 1.6 μg/m^3, and thus, 3 μg/m^3 was added to the ambient measurement values to adjust for this offset. The offset is a small fraction of the 10 h average $PM_{2.5}$ concentration (82 μg/m^3) during the smoke episode on 13 June 2012, though a significant fraction of 'background' concentrations.

A second technique for measuring $PM_{2.5}$ was the tapered element oscillating microbalance (Thermo Scientific Inc., model TEOM). TEOMs operated on the CSU Foothills campus [*Val Martin et al.*, 2013] and the CSU main campus providing hourly $PM_{2.5}$ concentrations. $PM_{2.5}$ on the main campus was operated as part of the Colorado Department of Public Health and Environment (CDPHE) ambient air quality monitoring program following Environmental Protection Agency protocols and calibration schedule.

Carbon monoxide (CO) was measured with a trace-level gas filter correlation nondispersive infrared absorption technique (Teledyne-API, Inc., Model 300EU). The instrument, housed in a mobile lab at the Foothills location, sampled ambient air through a 0.6 cm OD Teflon sample tube. The instrument calibration was periodically checked during the sampling period with zero air and injections of a known concentration of CO [*Prenni et al.*, 2014]. All gas phase measurements are reported as mixing ratio in parts per million or parts per billion by volume (ppm or ppb).

2.5. Particle Sizing Measurements

Particle number concentrations ($dN/d\log D_p$) as a function of electrical mobility diameters (D_p) were measured with a fast mobility particle sizer (FMPS, Model 3091, TSI Inc.) [*Mirme and Tamm*, 1991; *Tammet et al.*, 2002]. The FMPS, covering the size range of $5.6 < D_p < 560$ nm, was developed for source testing of engine emissions, i.e., high-concentration, rapidly changing conditions, also typical of biomass burning events. The FMPS was a logical choice to apply to the case of biomass smoke experiments where the conventional scanning mobility particle sizer (SMPS) is too slow (minutes for a scan over this size range) to capture rapid changes. The conventional optical particle counter (OPC) also has nonidealities as it is insensitive to particles with $D_p < 0.1$ μm, is problematic for highly light absorbing aerosols, and has low saturation limits for particle concentration [*Reid et al.*, 2005b].

The FMPS sampled continuously at a flow rate of 9.6 ± 0.3 lpm (nominal flow rate = 10 lpm) as verified throughout the measurements with an external flow standard (BIOS International, Inc., DryCal). The FMPS uses an array of ring electrometers that measure 1 s particle size distributions in 32 size bins in equal log spacing over the range $D_p = 5.6$ nm to 560 nm. The FMPS sampled directly through an electrically conductive inlet line and through a cyclone ($D_p < 1$ μm), with no further sample conditioning. For the ambient measurements, the inlet extended 2 m above the roof and was approximately 7 m in length consisting of 1 cm OD copper sampling line. The laboratory measurements used a 3 m length of 1 cm OD copper tubing directed into the sampling stack counter to the stack flow. Sample residence time between sampling point and measurement was <3 s in both cases. All plumbing between the sample inlet and instrument was stainless steel fittings (Swagelok, Inc.) and 1 cm OD electrically conductive tubing.

A number of studies have employed the FMPS instrument to examine highly variable and high-concentration particle size distributions, including a laboratory study of biomass smoke properties, biogenic emissions from a forest, and near-roadway emissions [*Hosseini et al.*, 2010; *Pryor et al.*, 2009; *Weimer et al.*, 2009]. The FMPS instrument demonstrated high correlations with the measurements of a standard SMPS (TSI, Inc., Model 3936) [*Asbach et al.*, 2009; *Price et al.*, 2014], though with some deviations. For example, fresh smoke aerosols contain sooty agglomerates that can complicate sizing measurements [*Leskinen et al.*, 2012; *Zimmerman et al.*, 2014], particularly with respect to impacts of relative humidity processing [*Lewis et al.*, 2009]. The impact of multiple charging with a unipolar diffusion charging in the FMPS is particularly acute for larger particles and more complex shapes [*Levin et al.*, 2015]. Due to the limitations observed here and in past studies of the FMPS technique for measuring larger accumulation mode particles, we refrain from assuming a density to use the integrated measurement as a proxy for $PM_{2.5}$ mass concentration. We show a semiquantitative aerosol volume to illustrate trends.

FMPS inlet temperature and humidity were monitored with a newly installed capacitive sensor, under factory calibration (Vaisala Inc., Humicap RH and Temperature Probe, HMP110) interfaced to the analog inputs of the FMPS instrument. The FMPS was monitored for many diagnostic parameters such as flow rates, voltages, and other parameters and generates exception errors for diagnostic parameters out of tolerance (TSI, Inc. FMPS 3091 User Manual). Routine cleaning of the classifier column occurred periodically and typically daily during the laboratory experiments. The instrument was run with particle free air periodically to confirm its zero measurement (Gelman Science, HEPA capsule filter PN 12144, 99.97% retention of 0.3 μm) and to rezero the electrometers as needed (daily and typically before each combustion experiment).

Ambient FMPS measurements were intended for consistency with the laboratory measurements rather than fast time response needs. The ambient particle size distribution measurement was located at the east Fort Collins site, while its sampling location during the laboratory measurements is shown in Figure 1. Lognormal particle sizing characteristics were calculated for the size distributions including geometric mean diameter (D_g) and geometric standard deviation (σ_g).

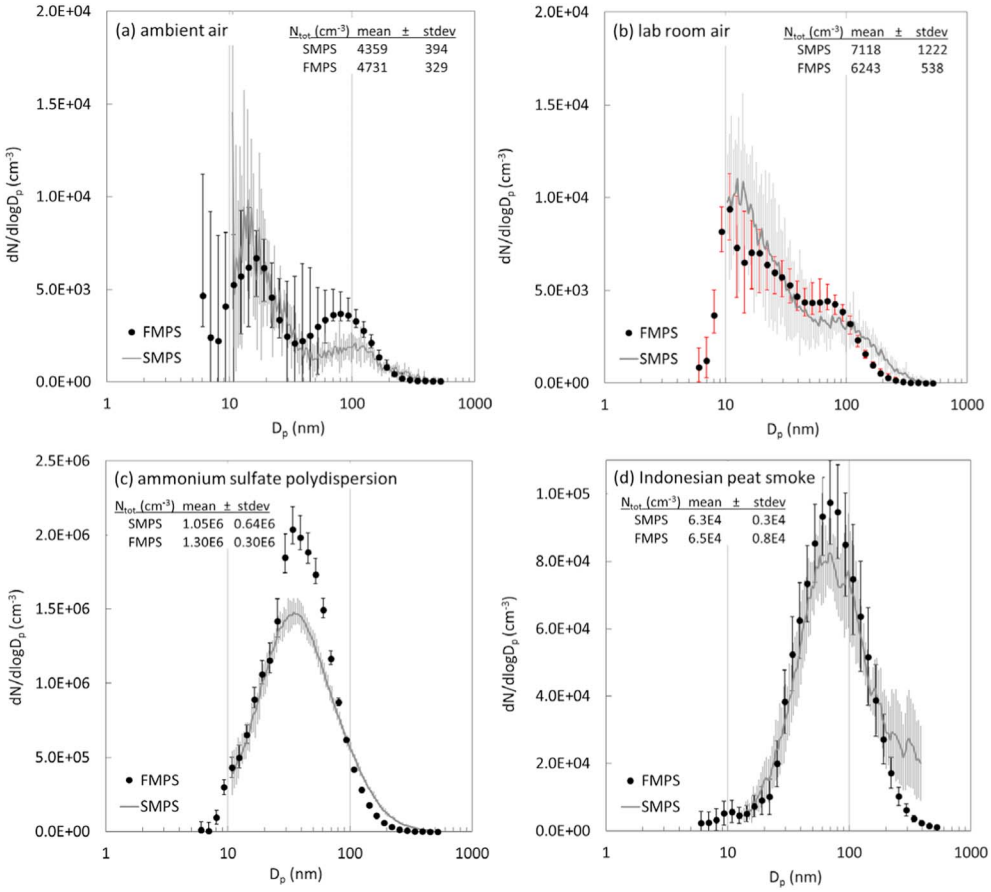

Figure 3. FMPS versus standard SMPS size distributions for (a) ambient air in Fort Collins, (b) room air at the Fire Science Lab in Missoula, MT, and (c) laboratory atomized ammonium sulfate polydispersion, and (d) slowly varying Indonesian Peak (FLAME-4 Burn 125). Bars show range of values for FMPS 1 s data and range of SMPS for approximately eight 5 min scans for the SMPS.

2.6. FMPS Measurement Quality Control Checks

Several tests were conducted to examine the response of the FMPS instrument in comparison to standards, including a scanning mobility particle sizer (TSI, Inc. SMPS Model 3081) and polystyrene latex spheres of known sizes (PSL, Duke Scientific Inc., USA). The series of measurements discussed here occurred during a 6 month period during which quality control checks were interspersed throughout the period demonstrating consistent instrument performance. The SMPS was run with standard firmware settings with 3–5 min voltage scan time and was fitted with a $D_p = 1$ μm impactor. Charge neutralization used a ^{85}Kr source (FLAME-4 combustion experiments) or a ^{210}Po source (laboratory pretesting), in each case within one half-life. The instrument was run with a flow ratio of 10:1, and SMPS software selections included multiple charging corrections.

The FMPS and its inversion scheme are intended for polydisperse aerosols, and these results are compared in more detail here. A comparison of particle size distributions from the FMPS versus SMPS instruments for polydisperse aerosols is shown in Figure 3 for two low- and two high-concentration cases: lab room air in Missoula during FLAME-4, ambient air in Fort Collins, a laboratory-generated polydispersion of ammonium sulfate (Fisher Scientific, Inc., reagent grade $(NH_4)_2SO_4$), and biomass smoke generated from laboratory combustion of Indonesian peat during FLAME-4. The Indonesian peat burn was a longer duration experiment with a fuel that smolders and thus slowly varied. The longer duration experiment and slow variability provided an opportunity to compare the FMPS response to the conventional, slower response SMPS method for polydisperse smoke.

Though the FMPS responds best to polydispersions as discussed, we also examined the instrument versus monodisperse aerosols generated with PSLs for thorough characterization. For PSLs in the range

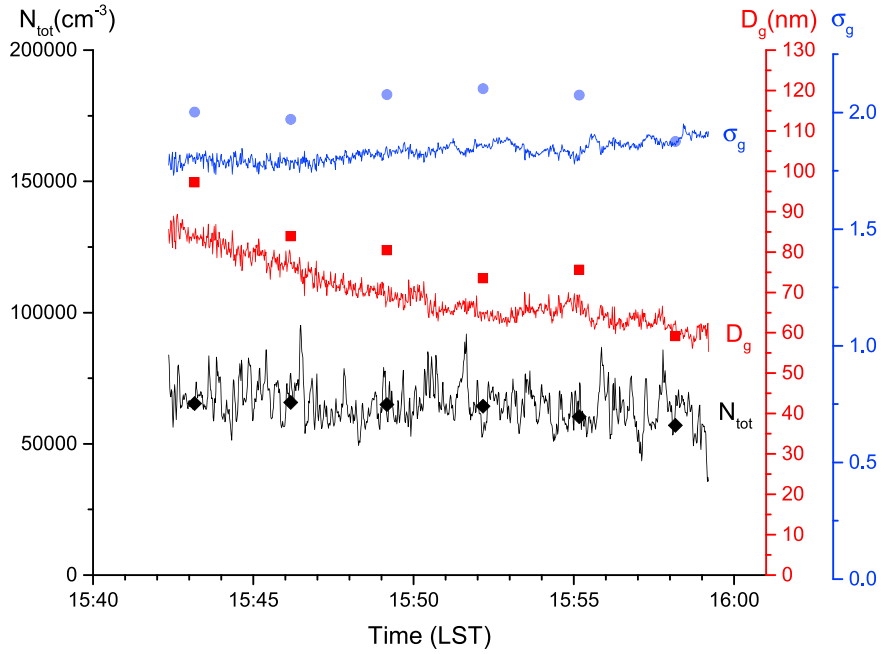

Figure 4. FMPS (solid lines) versus standard SMPS (markers) size distribution parameters (total number concentration, N_{tot}; geometric mean diameter, D_g; and geometric standard deviation, σ_g) over time for a slowly varying Indonesian peat (Burn 125) smoke measurement during FLAME-4.

of 50 nm $< D_p <$ 200 nm, several tests with monodisperse aerosols showed peaks in the FMPS size distribution within ±20% of the nominal size, though distributed more widely than an SMPS. For $D_p >$ 200 nm monodispersions, the FMPS lacked a clearly defined peak. This likely relates to both the lower concentration of monodisperse particles generated as well as the unipolar charging process of the instrument. The FMPS instrument, with seven size bins for $D_p >$ 200 nm, was less capable than an SMPS at resolving particles in this size range. Other investigators have likewise reported FMPS inaccuracies above $D_p =$ 200 nm [*Levin et al.*, 2015].

In addition to the lower size resolution compared to the SMPS, the FMPS instrument more often undersized versus oversized, consistent with PSL tests discussed earlier (Figure 3). The FMPS captured the bimodality of the ambient size distribution and room air, though there were discrepancies between the relative proportions as compared with the SMPS (Figure 3). Some of the larger particles may be sized into smaller size bins as suggested by the higher FMPS concentrations below $D_p =$ 100 nm in Figure 3. For these reasons, the measured sizing from the FMPS is likely a lower bound in terms of sizing D_p. Similar discrepancies have been noted in comprehensive laboratory intercomparisons [*Kaminski et al.*, 2013; *Lee et al.*, 2013]. The impacts of the unipolar diffusion charging in the FMPS were associated with this in other laboratory studies [*Levin et al.*, 2015]. A final comparison for sizing parameters as calculated for overlapping size ranges is shown for the slowly varying, smoldering Indonesian peat fuel (Figure 4). The burn progressed as a primarily smoldering burn throughout with no trend but rather small fluctuations in modified combustion efficiency (0.84 < MCE < 0.88). The sizing parameters N_{tot}, D_p, and σ_g agreed within ±20% and tracked the standard SMPS. Smaller D_p of the FMPS was largely due to the differences in measuring particles with $D_p >$ 200 nm as shown previously in Figure 3d. Although the higher accuracy, resolution and historical track record of the SMPS is acknowledged, the experiments show that for $D_p <$ 200 nm, the FMPS adequately captures the modality, approximate sizing characteristics, and concentrations of fresh biomass smoke in addition to the dynamic changes in these properties.

3. Results

3.1. Laboratory Biomass Smoke Measurements

Alaska black spruce demonstrated distinct combustion transitions and ensuing aerosol physical property impacts. A time series of physical properties shows the impacts of the transitions in combustion phase on

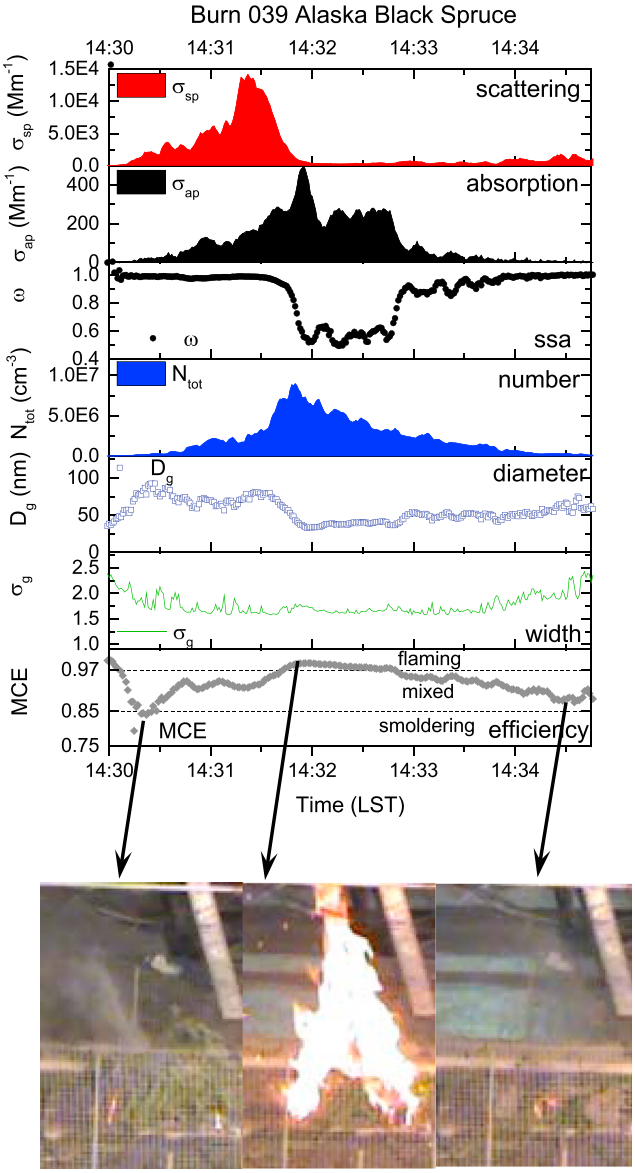

Figure 5. Time series of aerosol physical properties with representative FLAME-4 stack burns (Alaska black spruce, FLAME-4 Burn 039). Still images of the fire are shown at times 14:30:30, 14:32:00, and 14:35:00 (predominantly flaming, smoldering and flaming, respectively).

aerosol properties (Figure 5). Though biomass combustion is a spectrum of mixed flaming and smoldering, we differentiate in the figures approximate flaming (MCE > 0.97), mixed (0.85 < MCE < 0.97), and smoldering regimes (MCE < 0.85) [*Ward et al.*, 1996]. The burn began with a smolder phase reaching a minimum in MCE ~0.84; concurrently, a diameter peak approaching $D_p \sim 100$ nm occurred with ω approaching 1. By the time the fire reaches the full flaming stage with MCE > 0.97 around time 14:32 LST, peak number concentrations of strongly light absorbing particles were produced with ω approaching a minimum of ~0.5. An intensity plot of the number size distribution that is shown in Figure 6 illustrates the dynamic behavior in size distribution with the clear transition from smoldering to flaming around 14:32 LST along with a pronounced shift to smaller sizes. Though other parameters such as fuel matrix, composition, and moisture likely play a role, the cases shown here illustrate the importance of combustion phase in driving smoke aerosol properties.

For representative Ponderosa pine stack burn experiments (Burns 070 and 095, fuel mass = 274 and 150 g respectively), smoke measurements also demonstrated rapid shifts in size distribution with accompanying shifts in optical properties over the evolution of a biomass smoke experiment (Figure 7). Ponderosa pine burns had MCE = 0.917 + 0.032 (n = 15) with a range of 0.839 to 0.952; two burns were more smoldering with MCE < 0.9. FLAME-4 Burn 070 combusted mostly pine needles rather than a more typical mix of needles and branches. As a burn-average, Burn 070 featured MCE = 0.848, the second lowest MCE among Ponderosa pine burns, indicating its comparative smoldering nature. Two periods of flaming combustion are shown by two peaks in number concentration and corresponding peaks in MCE near the beginning of Burn 070. The size distribution shifted smaller during flaming combustion, with a particle number mode ~ D_p = 50 nm. Additionally, peaks in light absorption caused small declines in ω during the two lower MCE flaming periods. Smoldering combustion produced a strongly light scattering aerosol, dominated by particles with a number mode approximately $100 < D_p < 125$ nm. The transition to end-of-burn smoldering combustion featured a shift to a larger D_p and slightly wider mode with diminishing number concentrations.

All but two Ponderosa Pine burns had 0.9 < MCE < 0.95, and thus Burn 095 was more typical with MCE = 0.933. Burn 095 began with a smoldering phase, shifted toward flaming for 2 min and declined into a smoldering phase (Figure 7). Flaming dominance of Burn 095, indicated by its higher MCE, resulted in a

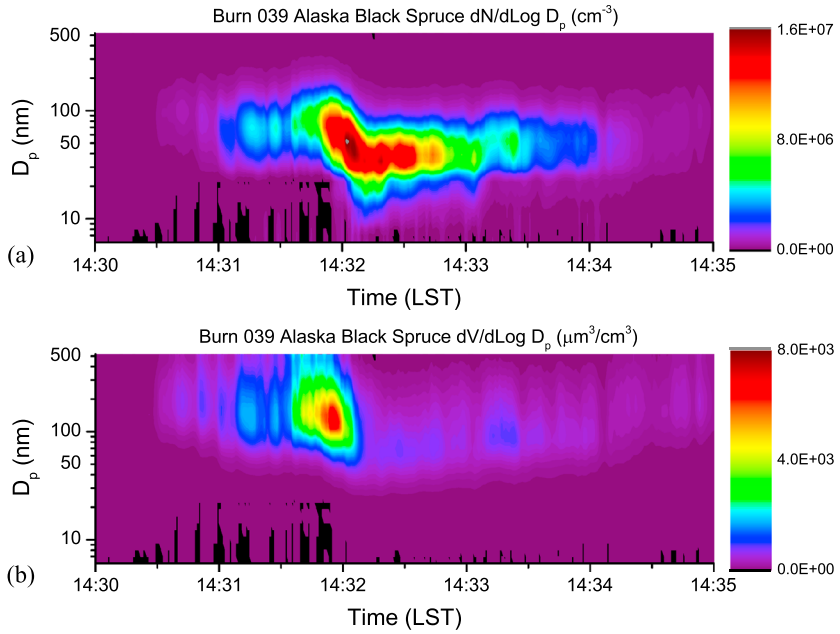

Figure 6. (a) Number and (c) volume size distribution intensity plots for FLAME-4 stack burn 039 with Alaska Black Spruce.

large number concentration of strongly absorbing particles ($N_{tot} = 1$ to $2(10)^6\,cm^{-3}$ for 2 min despite the smaller fuel mass than Burn 070). This is particularly evident at time 15:08:20 LST, as large number concentrations of highly absorbing particles with approximate $D_p = 50$ nm were emitted causing a decline in ω to 0.7 (Figure 7). A comparison of MCE, D_p and ω shows values of 0.87, 95 nm, and 0.99 during predominantly

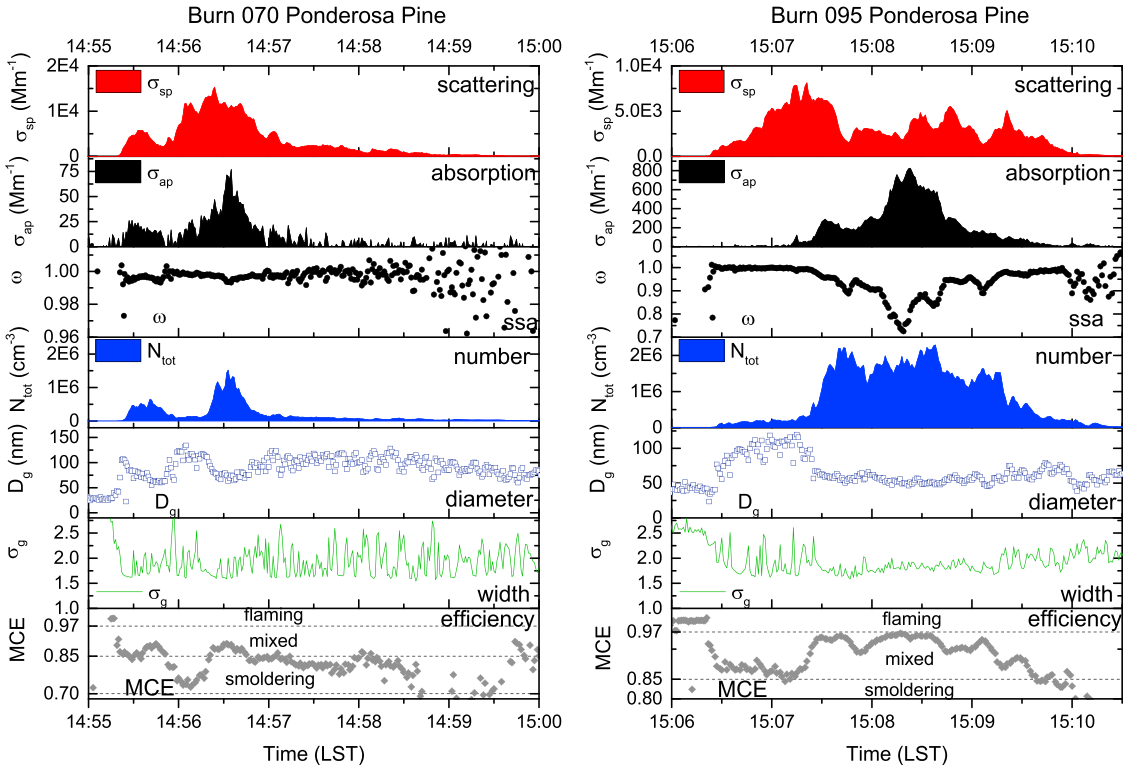

Figure 7. Time series of aerosol physical properties with representative FLAME-4 stack burns (Ponderosa pine FLAME-4 Burns 070 and 095).

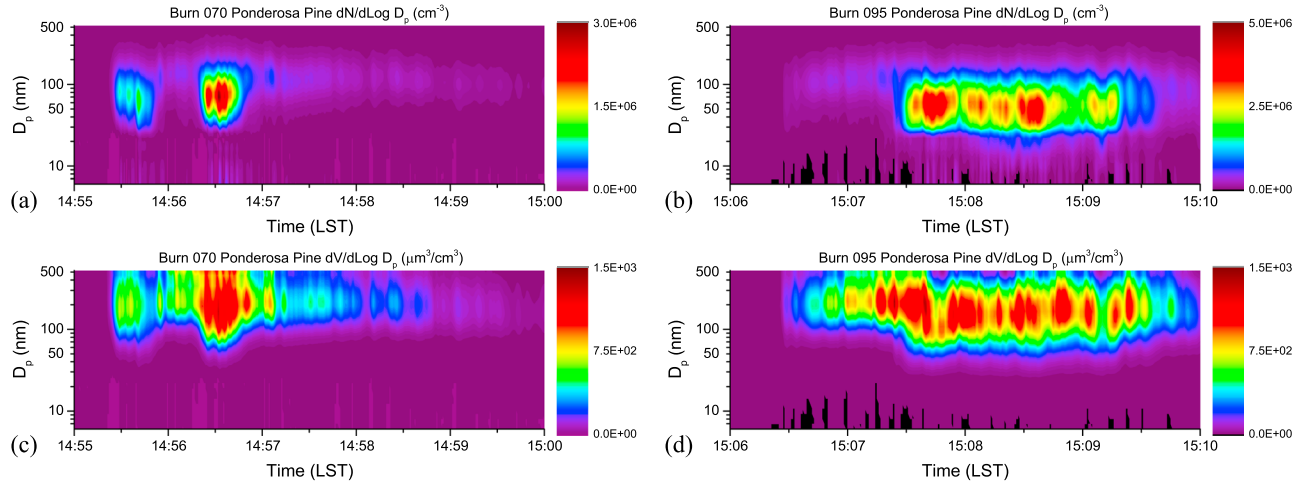

Figure 8. Number (a and b) and volume (c and d) size distribution intensity plots from representative FLAME-4 stack burns 070 and 095 with Ponderosa pine.

smoldering combustion from 15:06:30 to 15:07:30 versus 0.95, 55 nm, and 0.88, respectively, during the 90 s of predominantly flaming combustion that followed.

Size distribution intensity plots also show clear differences in burns 070 and 095. Two periods of flaming in burn 070 are illustrated by high number concentrations of smaller particles, coinciding with peaks in σ_{ap} (Figure 8). Burn 095 featured a single combustion phase transition, where smoldering dominated for the first minute of the burn followed by a peak in flaming combustion at approximately 15:38:30 LST, highlighted by the maximum in N_{tot} and σ_{ap} and minimum ω. Overall, a prominent feature in these data is the pronounced influence of combustion phase, i.e., the dominance of flaming versus smoldering phases, in driving both particle sizing and optical properties. A robust relationship between the MCE and ω was described across other FLAME-4 experiments with smoldering combustion characterized by low MCE and leading to high ω [*Liu et al.*, 2014].

The sampled smoke during room burns represented a mix of flaming and smoldering combustion with Ponderosa pine (Burn 140, 1672 g) as shown in Figure 9. Room burn experiments described here were nonilluminated experiments, differing from the photochemical smog chamber aging experiments that use an ultraviolet light source [*Grieshop et al.*, 2009]. The fire occurred over the first several minutes of the experiment, and early values of MCE indicated flaming influence. MCE reached a steady state in the mixed regime rapidly and remained steady for the remainder of the experiment (Figure 9). Sizing for Burn 140 showed number $D_p \sim 50$ nm during the beginning of the measurements and increased to $D_p \sim 100$ nm near the end of the 3 h sampling period while narrowing from $\sigma_g = 2.0$ to 1.6. This time frame of several hours is relevant as studies of biomass plumes in the atmosphere observed rapid changes in smoke microphysical properties over the first 2 h after emission [*Vakkari et al.*, 2014]. For Burn 140, a small to light scattering dominance was observed with $\omega < 0.9$ at the beginning and $\omega > 0.95$ by the end (Figure 9). Particle number concentration followed an exponential decay due to wall losses as well as coagulation. Light extinction declined exponentially, though less rapidly due to the shift in size distribution to larger D_p.

The smoke size range observed here is consistent with previous FLAME-2 laboratory measurements during the slowly changing room burns measured over 5 min time scales with a differential mobility particle sizing system, optical particle sizer, and aerodynamic particle sizer. Past results showed single number modes ranging from $D_g = 50$ to 140 nm and $\sigma_g = 1.6$ to 1.9, dependent on a wide range of fuel types and combustion [*Levin et al.*, 2010]. With respect to volume, some experiments demonstrated a second coarse mode captured by the aerodynamic particle sizer and attributed to smoldering combustion. No results were given for Ponderosa pine, though results were reported ($n = 4$) for two other western U.S. forest components Douglas fir and black spruce. These showed initial $D_p = 70$ to 80 nm and $\sigma_g = 1.64$ to 1.86 with D_p increasing modestly over the first hour after emission [*Levin et al.*, 2010].

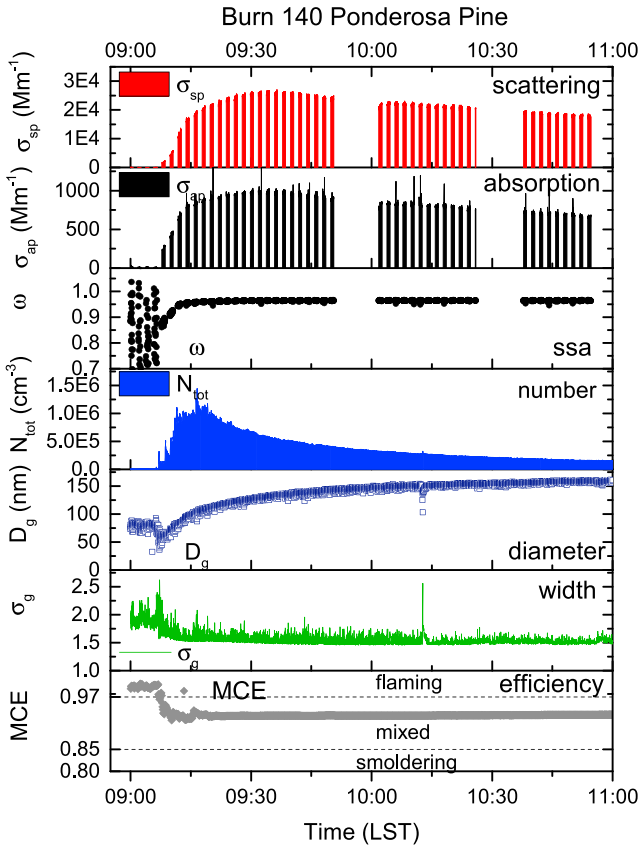

Figure 9. Representative FLAME-4 "room" burn (Burns 140) with Ponderosa pine. "Blank" periods in the optical traces are due to filtered zero air measurements.

3.2. Measured High Park Fire Biomass Smoke Properties

A summary of the period affected by smoke during the High Park Fire in June 2012 is shown in Figure 10, illustrating the high variability and episodic nature of smoke effects on air quality. We give the caveat that though these results are characteristic of these sampling conditions, they are not presumed to apply necessarily to other smoke events, particularly the extensive aerosol properties. Most sites and instruments exhibited approximately synchronous impacts during the events; however, the relative magnitudes and timing of each event shown in Figure 10 varied somewhat among instruments and sites. Here the focus is on the episode-wide properties, and the finer timescale variations in smoke aerosol properties likely differed due to different sampling sites coupled with the complex mountain topography of the burn area. Due to the mountain location and plume rise, the High Park Fire often produced a smoke plume lofted above the CFR region, particularly during enhanced daytime vertical convection. As confirmation, average plume height above the CFR during the High Park Fire was determined to be 4.4 km above the surface [*Val Martin et al.*, 2013]. Stable atmospheric conditions at night, depending on synoptic scale meteorology, allowed smoke from the fire to drain down into lower elevation sites including Fort Collins and the northern CFR. As a result, hourly $PM_{2.5}$ concentrations episodically varied between background concentrations and exceedances of 100 $\mu g/m^3$ depending on smoke plume hits. These diel trends were also noted in a study of ice nucleation by High Park Fire impacted aerosols [*McCluskey et al.*, 2014].

An example of a heavily smoke-impacted event occurred in the early morning hours on 13 June 2012 (Figure 11). The event typifies many of the other smoke events shown in Figure 10, occurring overnight and into the morning hours during times of decreased vertical convection and light winds. The event is examined here in detail as all instruments were operational during the event. Measurements at the four sites along the northern CFR showed heaviest smoke during the morning hours between approximately 01:00 and 12:00 LST. $PM_{2.5}$ at the three Fort Collins sites showed similar temporal trends with maximum measured hour average $PM_{2.5}$ at the main campus TEOM site exceeding 200 $\mu g/m^3$ at peak impact (Figure 11). The average CO concentrations before, during, and after the smoke event were 281, 1674, and 145 ppb, respectively, suggesting minor smoke or other combustion impacts before and possibly after the smoke episode.

FMPS-integrated aerosol volume concentrations (abbreviated here $PM_{0.56}$ volume) showed the second peak clearly (Figure 11), though the first peak was smaller at the more distant East Fort Collins site as shown in the integrated number concentration in Figure 12. During the smoke event period from approximately 01:00 to 12:00 LST on 13 June 2012, the TEOM $PM_{2.5}$ to PM_{10} ratios were 0.52 and 0.68 on the foothills and main campus, respectively, indicating a substantial coarse mode contribution to PM mass not captured by the FMPS. The considerable coarse mode contribution was also noted in *McCluskey et al.* [2014] as it related to mineral dust species and ice cloud nucleation. Though number concentrations were small, PM mass was likely significant from the aerosol population with $0.56 < D_p < 2.5$ μm. This, combined with the undersizing of larger

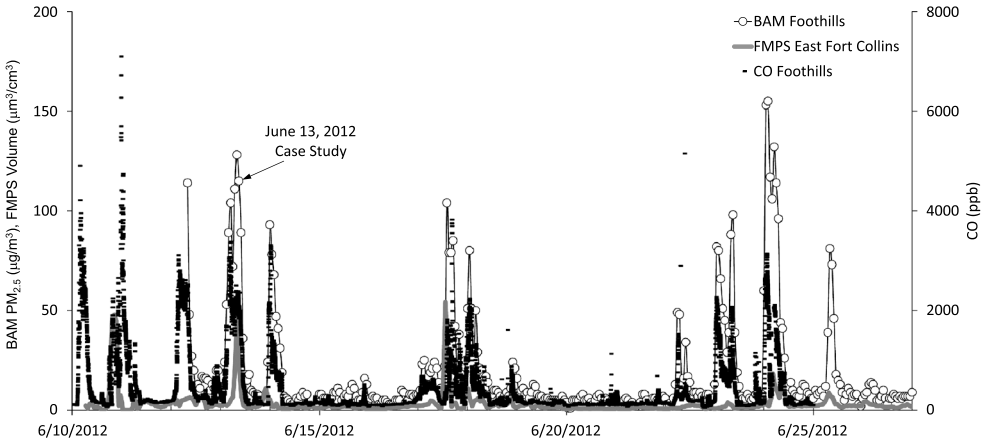

Figure 10. Measured ambient biomass smoke $PM_{2.5}$ mass concentration (BAM), volume concentration (FMPS), and carbon monoxide (CO) for a smoke-impacted period during the High Park Fire on 10–30 June 2012.

particles described above, means that FMPS-integrated volume concentrations were thus an underrepresentation of the true $PM_{2.5}$ volume. Carbon monoxide (CO) at the Foothills location reached a maximum 1 h value of 2.5 ppm at 05:00 LST, remaining elevated at approximately 2 ppm until 10:00 LST. By 14:00 LST, CO concentration declined to a typical background tropospheric concentration of 0.15 ppm. The smoke event ended as winds increased and shifted to southeasterly from 10:00 LST until 15:00 LST, increasing ventilation of the air shed from the direction opposite the fire.

Aerosol light scattering and absorption coefficients (σ_{sp} and σ_{ap}) and single scattering albedo (ω) are plotted in Figure 12 in comparison to particle sizing properties D_p, σ_g, and N_{tot} during the episode. Measurements of biomass smoke demonstrated rapid transitions in size and optical properties throughout the smoke event. A peak in particle number concentrations and light extinction occurred at approximately 07:45 LST on 13 June 2012. Before the event, the geometric number mean diameter was approximately $D_p = 50$ nm (Figure 12). As number concentration reached a peak of $N_{tot} = 2.7(10)^4\ cm^{-3}$, the distribution was unimodal reaching the event maximum of $D_p = 126$ nm at ~07:45 LST. The distribution also narrowed from $\sigma_g = 2.4$ before the event to $\sigma_g = 1.5$ during the event peak. The impacts of the sizing shift is evident in an increased aerosol volume scattering efficiency which was $16.4 \pm 13.9\ m^2\ cm^{-3}$ during the 11 h event versus $3.4 \pm 2.6\ m^2\ cm^{-3}$ in the 8 h after the event. The estimated volume scattering efficiency is based on measured light scattering and the integrated volume distribution, the latter of which is an underestimate due to FMPS nonidealities as

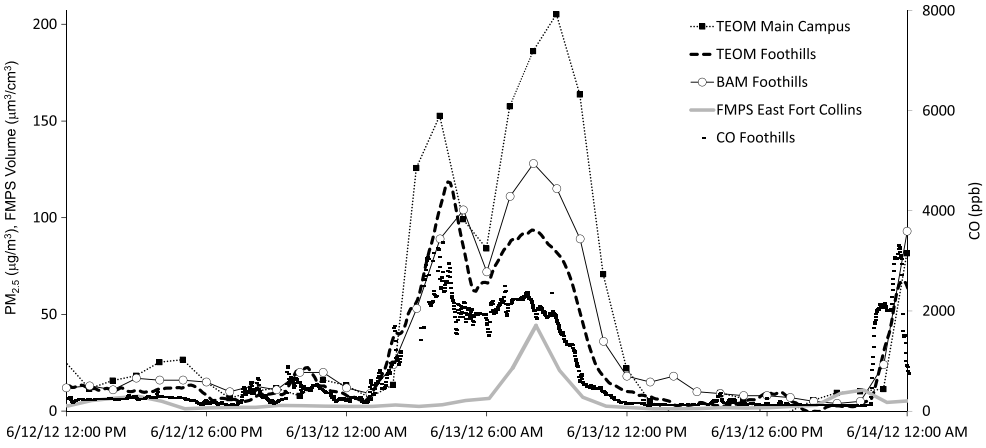

Figure 11. Measured ambient biomass smoke ambient particle size and optical properties for a smoke-impacted period during the High Park Fire on 13 June 2012.

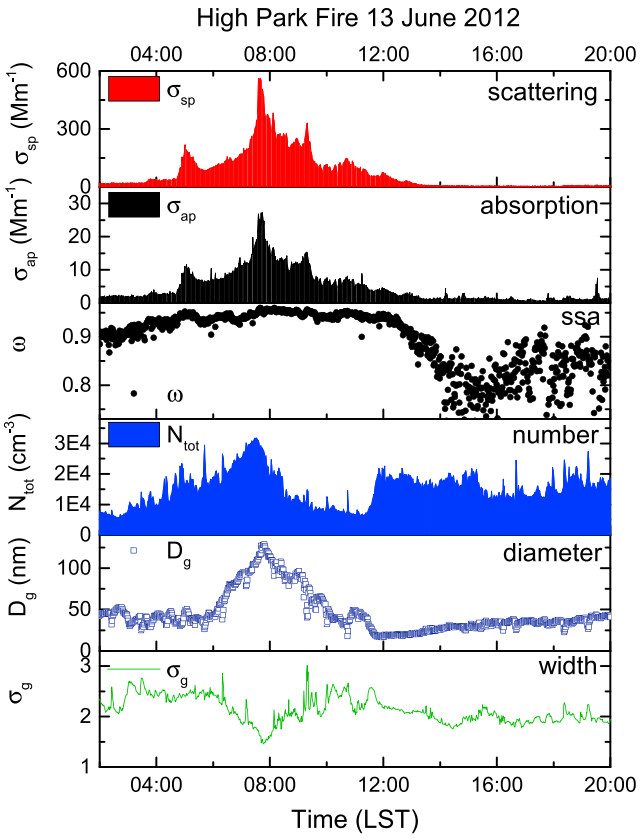

Figure 12. Measured ambient particle size (East Fort Collins site) and aerosol optical properties (Loveland site) for a smoke-impacted period (01:00–12:00 LST) during the High Park Fire on 13 June 2012.

discussed previously. Due to the stagnant winds and complex topography in the burn area, the age of the smoke during this event is difficult to ascertain, but it was likely hours to less than 1 day old due to the proximity of the sampling sites to the fire. We lacked a direct measurement of the flaming versus smoldering nature of the High Park Fire. For typical biomass burning events, the minimum in fire radiative energy is between 00:00 and 08:00 [*Vermote et al.*, 2009]. Due to lighter, downslope winds, increased stability, lower temperatures, and higher humidity, fire intensity typically decreases favoring smoldering combustion and drainage of smoke downslope [*Rothermel*, 1983]. These conditions prevailed here with subsidence of smoke from the mountains to Fort Collins which was facilitated by the light winds. Such behavior suggests a relatively greater smoldering influence in these overnight measurements compared with conditions later in the day.

As shown in Figure 12, large synchronous peaks in light absorption, light scattering, and single scattering albedo were observed at ~07:45 LST, with a peak light extinction coefficient of $\sigma_{ep} = 569 \pm 21\ \mathrm{Mm}^{-1}$ and peak single scattering albedo $\omega = 0.955 \pm 0.004$ (both 870 nm, 10 min average). For ω, an intensive property, this is only slightly higher than the 11 h episode average $\omega = 0.93 \pm 0.02$, as single scattering albedo remained high throughout the smoke episode, between 0.90 and 0.95. After 12:00 LST, with stronger winds from the southeast and convective mixing, light extinction dropped dramatically (Figure 12).

Measurements of High Park Fire smoke indicate a light scattering-dominated aerosol, consistent with preferentially smoldering combustion [*Liu et al.*, 2014]. The magnitude of light extinction is comparable to a polluted megacity as the dry light extinction coefficient in summertime Beijing, China was reported as 571 Mm^{-1} at a midvisible wavelength [*Bergin et al.*, 2001]. This is equivalent to a visual range $V_r = 3.3$ km using the Koschmieder relationship $V_r = 1.9/\sigma_{ep}$ [*Griffing*, 1980] (where the constant 1.9 has been given values ranging from 1.4 to 3.9 depending on the threshold sensitivity of the observer's eye). This also ignores any gas phase light extinction and the wavelength dependence of σ_{ep} which could lower V_r by a factor of 2 or more. These magnitudes are considerably higher than those measured in Yosemite National Park in 2002 where long-range transported smoke impacted the site with σ_{sp} (at 530 nm) reaching 200 Mm^{-1} [*McMeeking et al.*, 2006].

In Figure 13, size distributions ($D_p < 560$ nm) from the east Fort Collins site are shown in the form of number ($dN/d\log D_p$) and aerosol volume ($dV/d\log D_p$) intensity plots. These data show the dominance of a unimodal number mode with $D_p > 100$ nm during the peak of the smoke episode. Afterwards, during the afternoon of 13 June 2012 from 12:00–22:00 LST, number concentration remained relatively high ($N_{tot} = 17.4 \pm 2.6\ (10)^3\ \mathrm{cm}^{-3}$) though aerosol mass reached a minimum ($PM_{2.5} = 5.7 \pm 3.7\ \mu\mathrm{gm}^{-3}$ at the foothills site) (Figure 13). These events, dominated by D_p ~20 nm particles, were distinct as compared to the high $PM_{2.5}$ concentration smoke events where D_p ~ 100 nm dominated (Figure 14).

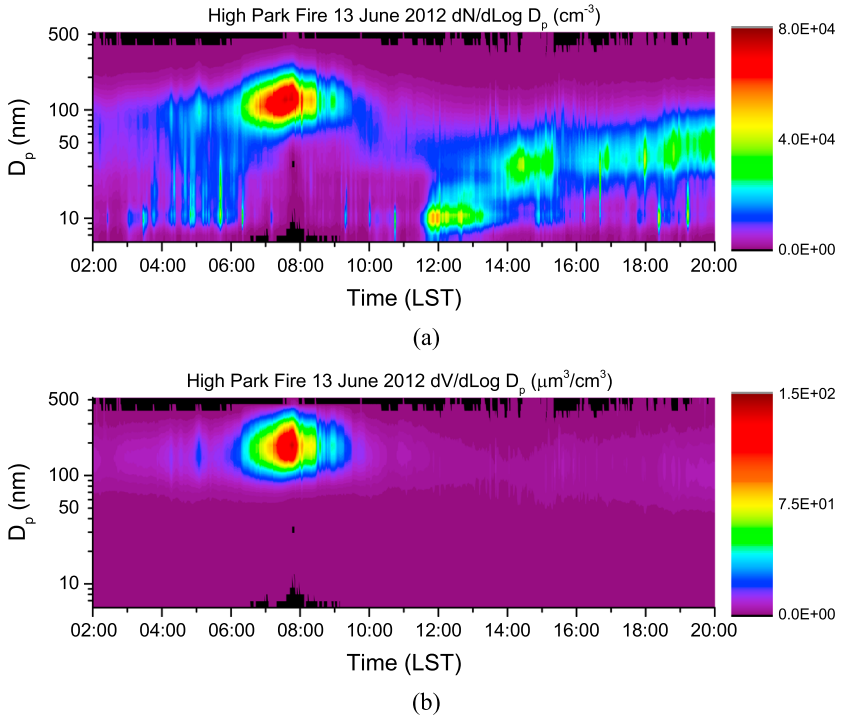

Figure 13. Measured ambient particle (a) number and (b) volume size distributions measured at the East Fort Collins site for a smoke-impacted period during the High Park Fire on 13 June 2012.

3.3. Western U.S. Aged Smoke Impacts

CDPHE measurements at the nearby CSU main campus site defined a smoke episode from approximately 15:00 LST on 14 August 2012 until 09:00 LST on 15 August 2012. Comparing presmoke episode (00:00–14:00 LST on 14 August 2012) versus smoke measurements shows $\sigma_{ep} = 113 \pm 27$ versus 244 ± 71 Mm^{-1}, $PM_{2.5} = 10 \pm 3$ versus 30 ± 10 μg/m^3, and CO = 164 ± 108 versus 210 ± 213 ppb. Compared to the High Park Fire episode, the aged smoke particle number distribution shows a more variable population of particles impacting the east Fort Collins site during the aged smoke episode (Figure 15). During the 19 h impacted by smoke shown on 14–15 August 2012, number and volume concentrations ($D_p < 560$ nm) ranged from $4000 < N_{tot} < 28{,}000$ cm^{-3} and $4 < V_{tot} < 9$ μm^3/cm^3. Combined with the expected much lower smoke concentrations than the High Park Fire, it is likely local sources contributed substantially, particularly the large number concentrations for ultrafine particles around rush hour at 08:00 LST on 15 August 2012 (Figure 15).

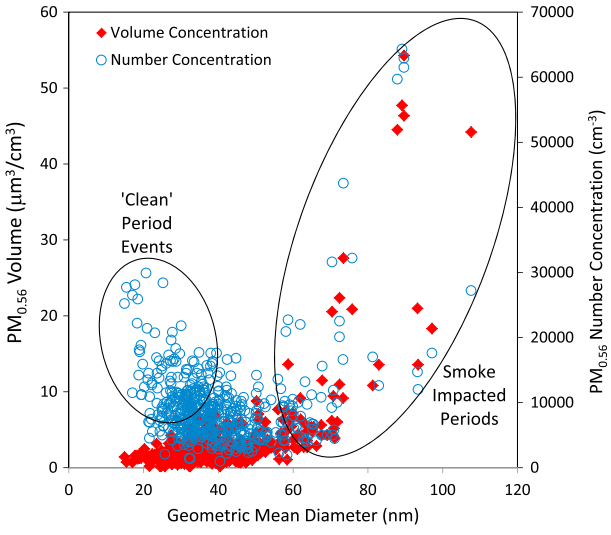

Figure 14. $PM_{0.56}$ volume and number concentrations versus geometric mean diameter on a 1 h average basis from 10–30 June 2012.

The event reached a peak around 16:00 LST on 14 August 14 with peak $\sigma_{ep} = 337$ Mm^{-1} and peak $PM_{2.5} = 61$ μg/m^3. During this period, the aged smoke number sizing parameters (2 h peak) were $N_{tot} = 3.6 \pm 1.5$ $(10)^3$ cm^{-3}, $D_p = 101 \pm 12$ nm, and $\sigma_g = 2.2 \pm 0.2$. This compares to the High Park Fire

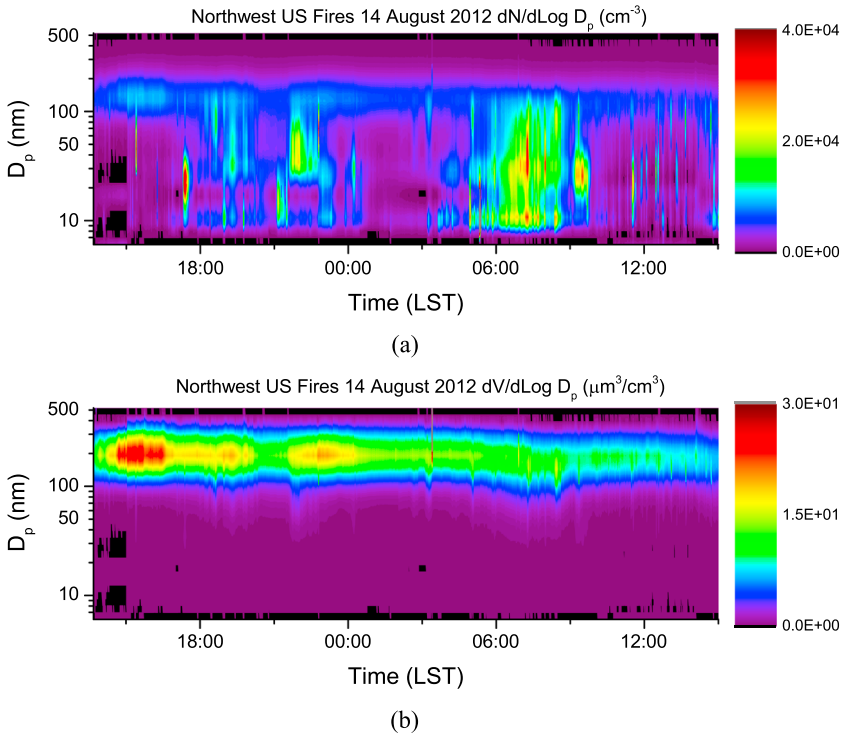

Figure 15. Ambient particle (a) number and (b) volume size distributions measured at the East Fort Collins, CO site on 14–15 August 2012 and impacted by long-range transported smoke from the northwestern U.S.

fresh smoke 2 h respective peak values of $N_{tot} = 23.9 \pm 5.6(10)^3$ cm^{-3}, $D_p = 99 \pm 14$ nm, and $\sigma_g = 1.8 \pm 0.2$. The aged smoke had a number maximum at $D_p = 143$ nm, also slightly larger than High Park Fire maximum at $D_p = 120$ nm. The wider aged distribution is due to the proportionally greater contributions of the population with $D_p < 100$ nm shown in Figure 15. Thus, the aged smoke had a size distribution shifted to slightly larger size with a wider distribution though generally similar to the much younger High Park Fire. Not surprisingly due to the effects of dilution, coagulation, and removal processes, total number concentration of the aged smoke is approximately a factor of 7 lower compared with the fresh emissions from the High Park Fire.

Examining the volume distribution, volume geometric mean diameters and standard deviations were $D_p = 190 \pm 5$ nm and $\sigma_g = 1.4 \pm 0.0$ versus $D_p = 180 \pm 5$ nm and $\sigma_g = 1.5 \pm 0.0$ for the aged smoke and High Park Fire 2 h maximum periods, respectively. These are slightly below those compiled in the review of biomass smoke by *Reid et al.* [2005a, 2005b] who reported a range of volume median diameters of $D_p = 210$ to 300 nm for biomass smoke using SMPS and OPC data. Likewise, during smoke-impacted measurements at a background location at Yosemite National Park in summer 2012, *McMeeking et al.* [2006] found long-range transported smoke characterized by volume mean $D_p = 320 \pm 40$ nm, $\sigma_g = 1.6$, and volume concentration of approximately 25 μm^3 cm^{-3}. Their measurements included a differential mobility particle sizer ($D_p < 0.85$ μm) and an optical particle counter (100 nm $< D_p <$ 2 μm). Applying an upper limit of $D_p < 560$ nm to *McMeeking et al.* [2005] data would result in missing roughly a third of the accumulation mode mass they observed. Thus, the FMPS upper size limit plus the undersizing of particles ($D_p > 200$ nm) combined to make FMPS-measured volume distribution properties likely a lower limit of true accumulation mode volume and mass concentration.

4. Discussion and Conclusion

Aerosol microphysical properties across this series of ambient and laboratory experiments showed dynamic response to combustion conditions as well as a consistent picture of smoke microphysical properties from emission to aging. Sizing ($D_p < 560$ nm) and aerosol optical properties observed show a distinct impact of

combustion phase (flaming versus smoldering) driving the size distribution of emitted particles. During lab experiments with Ponderosa pine and Alaskan black spruce, synchronous shifts to larger sizes and light scattering dominance were associated with the transition from flaming to smoldering combustion. From laboratory studies, flaming combustion (MCE $>$ 0.95) favored emission of a $D_p < 50$ nm particles with strongly light absorbing properties (ω at 870 nm as low as 0.5). The size distribution shifted to larger sizes (D_p approaching 100 nm) in the first few hours after emission. Smoldering combustion (MCE $<$ 0.95) emissions favored larger sizes ($D_p \sim 100$ nm) at the outset, while light scattering dominated light extinction ($\omega > 0.95$). Combustion phase was thus a key though not exclusive driver, with flaming combustion generally producing size distributions shifted toward smaller more absorbing particles compared to smoldering combustion which produced larger and light scattering-dominated aerosols.

In a smoke episode during the High Park Fire (hours old smoke), the size distribution featured a maximum in D_p, a minimum in width σ_g, and the optical measurements showed a maximum in ω. At the peak of a smoke episode during the High Park Fire, light extinction reached a maximum with $\sigma_{ep} = 569 \pm 21\ Mm^{-1}$ (870 nm, 10 min average) with aerosol single scattering albedo simultaneously peaking with $\omega = 0.955 \pm 0.004$, indicating a light scattering-dominated aerosol even for this relatively fresh smoke. Concurrently, aerosol sizing showed a maximum $N_{tot} = 2.7(10)^4\ cm^{-3}$ during the episode, unimodal with $D_p = 126$ nm and $\sigma_g = 1.5$. Thus, the peak in number concentration and light extinction corresponded to a maximum particle D_p and minimum width. The observed properties were most similar to a fire with a substantial smoldering component consistent with wildfires smoldering peak during early morning hours. Later in the season, an aged smoke-impacted period affected Fort Collins in mid-August 2012. The event was impacted by aged smoke-impacted air arriving from the northwest U.S. The days-old smoke sampled from western U.S. fires was quite similar in its sizing properties to the younger High Park Fire smoke, with D_p slightly larger though within 5% on both a number and volume basis. This underscores that much of the evolution occurred soon after emission as observed in the laboratory with experiments extending over several hours.

Biomass burning smoke impacts include human health concerns, visibility degradation, cloud and climate interactions, atmospheric chemistry impacts, and air quality regulatory compliance issues. Climatic changes to date as well as future projections underscore the growing impact of burn season length and regional drought conditions to wildland fire extent. Future projections of climate change portend increasing average burned acreage in the western U.S. and resultant air quality impacts. When viewed with respect to increasing prevalence of large-scale, high-intensity, crowning (flaming) wildfires, biomass burning aerosol properties such as the size and optical properties of the particle population emitted could be altered as a consequence [*Bessie and Johnson*, 1995; *Hessburg et al.*, 2005; *Westerling et al.*, 2011]. Aerosol microphysical properties examined here, including the particle size distribution and light scattering and absorption, are important determinants of aerosol radiative properties and other impacts. The results provide useful information for freshly emitted biomass combustion aerosols that can be used as model inputs for biomass smoke aerosol microphysical properties.

Acknowledgments
Data from this study is available by emailing the corresponding author (carrico@nmt.edu). This work was supported by the U.S. National Science Foundation under award AGS-1260371. The authors acknowledge the important contributions from U.S. Forest Service/U.S. Department of Agriculture Fire Science Laboratory in Missoula, MT, and logistical support provided under NASA Earth Science Division award NNX12AH17G.

References

Andreae, M. O., and P. Merlet (2001), Emission of trace gases and aerosols from biomass burning, *Global Biogeochem. Cycles*, *15*(4), 955–966, doi:10.1029/2000GB001382.

Arnott, W. P., H. Moosmuller, C. F. Rogers, T. F. Jin, and R. Bruch (1999), Photoacoustic spectrometer for measuring light absorption by aerosol: Instrument description, *Atmos. Environ.*, *33*(17), 2845–2852.

Arnott, W. P., H. Moosmuller, and J. W. Walker (2000), Nitrogen dioxide and kerosene-flame soot calibration of photoacoustic instruments for measurement of light absorption by aerosols, *Rev. Sci. Instrum.*, *71*(12), 4545–4552, doi:10.1063/1.1322585.

Asbach, C., H. Kaminski, H. Fissan, C. Monz, D. Dahmann, and S. Mülhopt (2009), Comparison of four mobility particle sizers with different time resolution for stationary exposure measurements, *J. Nanopart. Res.*, *11*(7), 1593–1609, doi:10.1007/s11051-009-9679-x.

Bergin, M., et al. (2001), Aerosol radiative, physical, and chemical properties in Beijing during June 1999, *J. Geophys. Res.*, *106*(D16), 17,969–17,980, doi:10.1029/2001JD900073.

Bessie, W. C., and E. A. Johnson (1995), The relative importance of fuels and weather on fire behavior in sub-alpine forests, *Ecology*, *76*(3), 747–762, doi:10.2307/1939341.

Bond, T. C., et al. (2013), Bounding the role of black carbon in the climate system: A scientific assessment, *J. Geophys. Res. Atmos.*, *118*, 5380–5552, doi:10.1002/jgrd.50171.

Carrico, C., M. Petters, S. Kreidenweis, A. Sullivan, G. McMeeking, E. Levin, G. Engling, W. Malm, and J. Collett (2010), Water uptake and chemical composition of fresh aerosols generated in open burning of biomass, *Atmos. Chem. Phys.*, *10*(11), 5165–5178, doi:10.5194/acp-10-5165-2010.

Certini, G. (2005), Effects of fire on properties of forest soils: A review, *Oecologia*, *143*(1), 1–10, doi:10.1007/s00442-004-1788-8.

Christian, T., B. Kleiss, R. Yokelson, R. Holzinger, P. Crutzen, W. Hao, B. Saharjo, and D. Ward (2003), Comprehensive laboratory measurements of biomass-burning emissions: 1. Emissions from Indonesian, African, and other fuels, *J. Geophys. Res.*, *108*(D23), 4719, doi:10.1029/2003JD003704.

Christian, T., B. Kleiss, R. Yokelson, R. Holzinger, P. Crutzen, W. Hao, T. Shirai, and D. Blake (2004), Comprehensive laboratory measurements of biomass-burning emissions: 2. First intercomparison of open-path FTIR, PTR-MS, and GC- MS/FID/ECD, *J. Geophys. Res.*, *109*, D02311, doi:10.1029/2003JD003874.

Grieshop, A., J. Logue, N. Donahue, and A. Robinson (2009), Laboratory investigation of photochemical oxidation of organic aerosol from wood fires. 1: Measurement and simulation of organic aerosol evolution, *Atmos. Chem. Phys.*, *9*(4), 1263–1277.

Griffing, G. W. (1980), Relations between the prevailing visibility, nephelometer scattering coefficient and Sun-photometer turbidity coefficient, *Atmos. Environ.*, *14*(5), 577–584, doi:10.1016/0004-6981(80)90089-x.

Hand, J., et al. (2005), Optical, physical, and chemical properties of tar balls observed during the Yosemite Aerosol Characterization Study, *J. Geophys. Res.*, *110*, D21210, doi:10.1029/2004JD005728.

Hessburg, P. F., J. K. Agee, and J. F. Franklin (2005), Dry forests and wildland fires of the inland Northwest USA: Contrasting the landscape ecology of the pre-settlement and modem eras, *For. Ecol. Manage.*, *211*(1–2), 117–139, doi:10.1016/j.foreco.2005.02.016.

Hosseini, S., Q. Li, D. Cocker, D. Weise, A. Miller, M. Shrivastava, J. Miller, S. Mahalingam, M. Princevac, and H. Jung (2010), Particle size distributions from laboratory-scale biomass fires using fast response instruments, *Atmos. Chem. Phys.*, *10*(16), 8065–8076, doi:10.5194/acp-10-8065-2010.

Jaffe, D., D. Chand, W. Hafner, A. Westerling, and D. Spracklen (2008), Influence of fires on O_3 concentrations in the western US, *Environ. Sci. Technol.*, *42*(16), 5885–5891, doi:10.1021/es800084k.

Kaminski, H., et al. (2013), Comparability of mobility particle sizers and diffusion chargers, *J. Aerosol Sci.*, *57*, 156–178, doi:10.1016/j.jaerosci.2012.10.008.

Kaufman, Y. J., and R. S. Fraser (1997), The effect of smoke particles on clouds and climate forcing, *Science*, *277*(5332), 1636–1639, doi:10.1126/science.277.5332.1636.

Kershaw, L., A. MacKinnon, and J. Pojar (1998), *Plants of the Rocky Mountains*, Lone Pine Publishing, Edmonton, CA.

Kreidenweis, S., L. Remer, R. Bruintjes, and O. Dubovik (2001), Smoke aerosol from biomass burning in Mexico: Hygroscopic smoke optical model, *J. Geophys. Res.*, *106*(D5), 4831–4844, doi:10.1029/2000JD900488.

Lang-Yona, M., Y. Rudich, E. Segre, E. Dinar, and A. Abo-Riziq (2009), Complex refractive indices of aerosols retrieved by continuous wave-cavity ring down aerosol spectrometer, *Anal. Chem.*, *81*(5), 1762–1769, doi:10.1021/ac8017789.

Lee, B. P., Y. J. Li, R. C. Flagan, C. Lo, and C. K. Chan (2013), Sizing characterization of the fast-mobility particle sizer (FMPS) against SMPS and HR-ToF-AMS, *Aerosol Sci. Technol.*, *47*(9), 1030–1037, doi:10.1080/02786826.2013.810809.

Leskinen, J., J. Joutsensaari, J. Lyyranen, J. Koivisto, J. Ruusunen, M. Jarvela, T. Tuomi, K. Hameri, A. Auvinen, and J. Jokiniemi (2012), Comparison of nanoparticle measurement instruments for occupational health applications, *J. Nanopart. Res.*, *14*(2), 16, doi:10.1007/s11051-012-0718-7.

Levin, E., et al. (2010), Biomass burning smoke aerosol properties measured during Fire Laboratory at Missoula Experiments (FLAME), *J. Geophys. Res.*, *115*, D18210, doi:10.1029/2009JD013601.

Levin, M., A. Gudmundsson, J. H. Pagels, M. Fierz, K. Molhave, J. Londahl, K. A. Jensen, and I. K. Koponen (2015), Limitations in the use of unipolar charging for electrical mobility sizing instruments: A study of the fast mobility particle sizer, *Aerosol Sci. Technol.*, *49*(8), 556–565, doi:10.1080/02786826.2015.1052039.

Lewis, K., et al. (2009), Reduction in biomass burning aerosol light absorption upon humidification: roles of inorganically-induced hygroscopicity, particle collapse, and photoacoustic heat and mass transfer, *Atmos. Chem. Phys.*, *9*(22), 8949–8966.

Liu, S., et al. (2014), Aerosol single scattering albedo dependence on biomass combustion efficiency: Laboratory and field studies, *Geophys. Res. Lett.*, *41*, 742–748, doi:10.1002/2013GL058392.

McCluskey, C., P. DeMott, A. Prenni, E. Levin, G. McMeeking, A. Sullivan, T. Hill, S. Nakao, C. Carrico, and S. Kreidenweis (2014), Characteristics of atmospheric ice nucleating particles associated with biomass burning in the US: Prescribed burns and wildfires, *J. Geophys. Res. Atmos.*, *119*, 10,458–10,470, doi:10.1002/2014JD021980.

McMeeking, G., et al. (2006), Smoke-impacted regional haze in California during the summer of 2002, *Agric. Forest Meteorol.*, *137*(1–2), 25–42, doi:10.1016/j.agrformet.2006.01.011.

McMeeking, G., et al. (2009), Emissions of trace gases and aerosols during the open combustion of biomass in the laboratory, *J. Geophys. Res.*, *114*, D19210, doi:10.1029/2009JD011836.

McMeeking, G. R., S. M. Kreidenweis, C. M. Carrico, T. Lee, J. L. Collett Jr., and W. C. Malm (2005), Observations of smoke-influenced aerosol during the Yosemite Aerosol Characterization Study: Size distributions and chemical composition, *J. Geophys. Res.*, *110*, D09206, doi:10.1029/2004JD005389.

Mirme, A., and E. Tamm (1991), Comparison of sequential and parallel measurement principles in aerosol spectrometry, *J. Aerosol Sci.*, *22*, S331–S334, doi:10.1016/s0021-8502(05)80105-3.

Naeher, L. P., M. Brauer, M. Lipsett, J. T. Zelikoff, C. D. Simpson, J. Q. Koenig, and K. R. Smith (2007), Woodsmoke health effects: A review, *Inhalation Toxicol.*, *19*(1), 67–106, doi:10.1080/08958370600985875.

Nakayama, T., H. Suzuki, S. Kagamitani, Y. Ikeda, A. Uchiyama, and Y. Matsumi (2015), Characterization of a three wavelength photoacoustic soot spectrometer (PASS-3) and a photoacoustic extinctiometer (PAX), *J. Meteorol. Soc. Jpn.*, *93*(2), 285–308, doi:10.2151/jmsj.2015-016.

National Oceanic and Atmospheric Administration (September 2012), State of the climate: Wildfires for august 2012, edited, National Climatic Data Center, http://www.ncdc.noaa.gov/sotc/fire/201208.

Noss, R. F., J. F. Franklin, W. L. Baker, T. Schoennagel, and P. B. Moyle (2006), Managing fire-prone forests in the western United States, *Front. Ecol. Environ.*, *4*(9), 481–487, doi:10.1890/1540-9295(2006)4[481:mffitw]2.0.co;2.

Park, R., D. Jacob, and J. Logan (2007), Fire and biofuel contributions to annual mean aerosol mass concentrations in the United States, *Atmos. Environ.*, *41*(35), 7389–7400, doi:10.1016/j.atmosenv.2007.05.061.

Pierce, J., G. Meyer, and A. Jull (2004), Fire-induced erosion and millennialscale climate change in northern ponderosa pine forests, *Nature*, *432*(7013), 87–90, doi:10.1038/nature03058.

Pope, C., and D. Dockery (2006), Health effects of fine particulate air pollution: Lines that connect, *J. Air Waste Manage.*, *56*(6), 709–742.

Posfai, M., A. Gelencser, R. Simonics, K. Arato, J. Li, P. Hobbs, and P. Buseck (2004), Atmospheric tar balls: Particles from biomass and biofuel burning, *J. Geophys. Res.*, *109*, D06213, doi:10.1029/2003JD004169.

Prenni, A., et al. (2014), Gas-phase reactive nitrogen near Grand Teton National Park: Impacts of transport, anthropogenic emissions, and biomass burning, *Atmos. Environ.*, *89*, 749–756, doi:10.1016/j.atmosenv.2014.03.017.

Price, H. D., B. Stahlmecke, R. Arthur, H. Kaminski, J. Lindermann, E. Dauber, C. Asbach, T. A. J. Kuhlbusch, K. A. BeruBe, and T. P. Jones (2014), Comparison of instruments for particle number size distribution measurements in air quality monitoring, *J. Aerosol Sci.*, *76*, 48–55, doi:10.1016/j.jaerosci.2014.05.001.

Pryor, S., R. Barthelmie, A. Spaulding, S. Larsen, and A. Petroff (2009), Size-resolved fluxes of sub-100-nm particles over forests, *J. Geophys. Res.*, *114*, D18212, doi:10.1029/2009JD012248.

Reid, J., T. Eck, S. Christopher, R. Koppmann, O. Dubovik, D. Eleuterio, B. Holben, E. Reid, and J. Zhang (2005a), A review of biomass burning emissions. Part III: Intensive optical properties of biomass burning particles, *Atmos. Chem. Phys.*, *5*, 827–849.

Reid, J., R. Koppmann, T. Eck, and D. Eleuterio (2005b), A review of biomass burning emissions. Part II: Intensive physical properties of biomass burning particles, *Atmos. Chem. Phys.*, *5*, 799–825.

Rocca, M. E., P. M. Brown, L. H. MacDonald, and C. M. Carrico (2014), Climate change impacts on fire regimes and key ecosystem services in Rocky Mountain forests, *For. Ecol. Manage.*, *327*, 290–305, doi:10.1016/j.foreco.2014.04.005.

Rothermel, R. C. (1983), How to predict the spread and intensity of forest and range fires, *Rep.*, United States Department of Agriculture Forest Service, Intermountain Forest and Range Experiment Station, Ogden, UT 84401.

Safford, H. D. (2013), Natural range of variation (NRV) for yellow pine and mixed conifer forests in the bioregional assessment area, including the Sierra Nevada, southern Cascades, and Modoc and Inyo National Forests, *Rep.*, USDA Forest Service, Pacific Southwest Region, Vallejo, CA.

Saleh, R., et al. (2014), Brownness of organics in aerosols from biomass burning linked to their black carbon content, *Nat. Geosci.*, *7*(9), 647–650, doi:10.1038/ngeo2220.

Spracklen, D., J. Logan, L. Mickley, R. Park, R. Yevich, A. Westerling, and D. Jaffe (2007), Wildfires drive interannual variability of organic carbon aerosol in the western US in summer, *Geophys. Res. Lett.*, *34*, L16816, doi:10.1029/2007GL030037.

Spracklen, D., L. Mickley, J. Logan, R. Hudman, R. Yevich, M. Flannigan, and A. Westerling (2009), Impacts of climate change from 2000 to 2050 on wildfire activity and carbonaceous aerosol concentrations in the western United States, *J. Geophys. Res.*, *114*, D20301, doi:10.1029/2008JD010966.

Stockwell, C., R. Yokelson, S. Kreidenweis, A. Robinson, P. DeMott, R. Sullivan, J. Reardon, K. Ryan, D. Griffith, and L. Stevens (2014), Trace gas emissions from combustion of peat, crop residue, domestic biofuels, grasses, and other fuels: Configuration and Fourier transform infrared (FTIR) component of the fourth Fire Lab at Missoula Experiment (FLAME-4), *Atmos. Chem. Phys.*, *14*(18), 9727–9754, doi:10.5194/acp-14-9727-2014.

Tammet, H., A. Mirme, and E. Tamm (2002), Electrical aerosol spectrometer of Tartu University, *Atmos. Res.*, *62*(3–4), 315–324, doi:10.1016/s0169-8095(02)00017-0.

Toth, A., A. Hoffer, I. Nyiro-Kosa, M. Posfai, and A. Gelencser (2014), Atmospheric tar balls: Aged primary droplets from biomass burning?, *Atmos. Chem. Phys.*, *14*(13), 6669–6675, doi:10.5194/acp-14-6669-2014.

Vakkari, V., et al. (2014), Rapid changes in biomass burning aerosols by atmospheric oxidation, *Geophys. Res. Lett.*, *41*, 2644–2651, doi:10.1002/2014GL059396.

Val Martin, M., C. Heald, B. Ford, A. Prenni, and C. Wiedinmyer (2013), A decadal satellite analysis of the origins and impacts of smoke in Colorado, *Atmos. Chem. Phys.*, *13*(15), 7429–7439, doi:10.5194/acp-13-7429-2013.

Val Martin, M., C. L. Heald, J. F. Lamarque, S. Tilmes, L. K. Emmons, and B. A. Schichtel (2015), How emissions, climate, and land use change will impact mid-century air quality over the United States: A focus on effects at national parks, *Atmos. Chem. Phys.*, *15*(5), 2805–2823, doi:10.5194/acp-15-2805-2015.

Veblen, T., T. Kitzberger, and J. Donnegan (2000), Climatic and human influences on fire regimes in ponderosa pine forests in the Colorado Front Range, *Ecol. Appl.*, *10*(4), 1178–1195, doi:10.2307/2641025.

Vermote, E., E. Ellicott, O. Dubovik, T. Lapyonok, M. Chin, L. Giglio, and G. Roberts (2009), An approach to estimate global biomass burning emissions of organic and black carbon from MODIS fire radiative power, *J. Geophys. Res.*, *114*, D18205, doi:10.1029/2008JD011188.

Ward, D., W. Hao, R. Susott, R. Babbitt, R. Shea, J. Kauffman, and C. Justice (1996), Effect of fuel composition on combustion efficiency and emission factors for African savanna ecosystems, *J. Geophys. Res.*, *101*(D19), 23,569–23,576, doi:10.1029/95JD02595.

Watson, J. (2002), Visibility: Science and regulation, *J. Air Waste Manage.*, *52*(6), 628–713.

Weimer, S., C. Mohr, R. Richter, J. Keller, M. Mohr, A. S. H. Prevot, and U. Baltensperger (2009), Mobile measurements of aerosol number and volume size distributions in an Alpine valley: Influence of traffic versus wood burning, *Atmos. Environ.*, *43*(3), 624–630, doi:10.1016/j.atmosenv.2008.10.034.

Westerling, A., H. Hidalgo, D. Cayan, and T. Swetnam (2006), Warming and earlier spring increase western US forest wildfire activity, *Science*, *313*(5789), 940–943, doi:10.1126/science.1128834.

Westerling, A., M. Turner, E. Smithwick, W. Romme, and M. Ryan (2011), Continued warming could transform Greater Yellowstone fire regimes by mid-21st century, *Proc. Natl. Acad. Sci. U.S.A.*, *108*(32), 13,165–13,170, doi:10.1073/pnas.1110199108.

Williams, A. P., C. D. Allen, C. I. Millar, T. W. Swetnam, J. Michaelsen, C. J. Still, and S. W. Leavitt (2010), Forest responses to increasing aridity and warmth in the southwestern United States, *Proc. Natl. Acad. Sci. U.S.A.*, *107*(50), 21,289–21,294, doi:10.1073/pnas.0914211107.

Wotawa, G., and M. Trainer (2000), The influence of Canadian forest fires on pollutant concentrations in the United States, *Science*, *288*(5464), 324–328, doi:10.1126/science.288.5464.324.

Yokelson, R., D. Griffith, and D. Ward (1996), Open-path Fourier transform infrared studies of large-scale laboratory biomass fires, *J. Geophys. Res.*, *101*(D15), 21,067–21,080, doi:10.1029/96JD01800.

Yokelson, R., et al. (2013), Coupling field and laboratory measurements to estimate the emission factors of identified and unidentified trace gases for prescribed fires, *Atmos. Chem. Phys.*, *13*(1), 89–116, doi:10.5194/acp-13-89-2013.

Zimmerman, N., K. J. G. Pollitt, C. H. Jeong, J. M. Wang, T. Jung, J. M. Cooper, J. S. Wallace, and G. J. Evans (2014), Comparison of three nanoparticle sizing instruments: The influence of particle morphology, *Atmos. Environ.*, *86*, 140–147, doi:10.1016/j.atmosenv.2013.12.023.